The Modular Loading and Unloading Structure for Logistics Drone

Zelu Chen

Brunel London School, North China University of Technology, Beijing, 100144, China

2282173@brunel.ac.uk

Abstract. In recent years, the low-altitude economy has developed rapidly, and the logistics industry is part of the low-altitude economy. The low-altitude logistics industry is also a part of the low-altitude economy. This study has designed a new structure of loading and unloading that can be used on the logistic drone, providing a reference for similar projects. The structure of loading and unloading is the essential component and the challenge of the logistics drone. The study will model the structure and simulate the fluid field and the structural strength of the structure. The results indicate that the new droplet-like low-resistance shell of the structure will optimize the wind resistance coefficient, reduce the energy consumption of the logistics drone, and ensure the structural strength at the normal cruising speed. The storage rack of the structure enables a more flexible cargo capacity without affecting the operation of the UAV and ensures structural integrity and a certain degree of stability.

Keywords: Logistics drone, Loading structure, Modular design.

1. Introduction

Nowadays, several major countries in the world, such as the United States, the United Kingdom and Germany, have accelerated the process of developing a low-altitude economy [1]. "Low-altitude economy" became a hot topic in China's civil aviation research in 2024, and has stimulated the development of the low-altitude logistics industry. The low-altitude logistics industry can effectively solve the problem of the "last mile" in the logistics sector [2]. With the integration of unmanned driving with transportation and logistics, coupled with the development of data cloud technology. Gradually form an integrated application. It can provide a faster and more convenient data transmission path for unmanned transportation [3]. By abandoning the two-dimensional ground road network distribution and shifting to three-dimensional logistics drones for cargo delivery, it can achieve this goal [4].

Since Google launched the Project Wing logistics drone project in 2012 [5], more companies both at home and abroad have begun to explore the field of logistics drones. Some of these models have been transformed from manned aircraft into unmanned ones. Meanwhile, companies like JINGDONG have redesigned the fuselage and cargo compartments to meet a wider range of usage requirements [6].

The medium-sized logistics drones should have a modular cargo compartment structure that can stably transport multiple small items, minimize air resistance, and be adaptable to various types of logistics drones. Because most of the medium-sized logistics drones adopt the air-hanging system to lift and transport goods, it will interfere with the buildings and the lives of citizens in the city. Low air resistance can further reduce the energy consumption of the unmanned aerial vehicle, enabling it to increase its operational efficiency. This modular logistics drone loading structure is designed to redesign a new type of cargo loading structure that can be installed on different logistics drones, has the ability to transport goods, and can reduce certain wind resistance.

2. Methods

2.1. Functional Requirements

To complete logistics tasks such as delivering parcels in urban areas and address the ‘last mile’ challenge in the logistics industry. This loading system should accommodate the transportation of goods of various sizes and facilitate future equipment maintenance. The loading structure should adopt a modular, interchangeable design. When transporting smaller goods, the system should enable the efficient delivery of multiple small items on a single trip. Additionally, each item must be accessible individually to ensure users can retrieve only their own packages. To accommodate different cargo sizes, the loading mechanism for small cargo should feature storage compartments of varying sizes to optimize space utilization and accommodate different dimensions of small cargo. It should also ensure the stability of items during transport to prevent swaying, which could affect the flight of the logistics drone.

2.2. Design Principles

Firstly, for the design of a loading structure capable of accommodating multiple small goods, it is essential to ensure that it can accommodate goods of various sizes and specifications, thereby achieving a certain degree of versatility. Additionally, each item should be capable of independent retrieval, allowing users to directly store and retrieve goods. Furthermore, the top or sides of the loading structure should have modular connection points for logistics drones, ensuring a secure connection that cannot be arbitrarily disassembled or reassembled by unauthorized personnel. The type of modular loading structures should feature low-drag shells to minimize interference from sudden gusts during drone flight. They should also be constructed using lightweight, high-strength materials to reduce the structure's self-weight, enabling the transport of heavier cargo loads. The power supply for the loading structures should not utilize the power source from the logistics drone, but instead adopt a replaceable battery solution. This approach significantly enhances the flexibility of the loading structure and is suitable for simultaneous use across multiple logistics drones.

2.3. Structural Design

Based on the above design principles, assuming that this modular loading structure will be installed on Phoenix Wings Company's Ark 150 medium-sized logistics drone, the dimensions of the loading structure will be designed based on the dimensions of the Ark 150 medium-sized logistics drone. To meet the low wind resistance design requirements, the outer shell structure of the loading structure will adopt a water drop-shaped low wind resistance design. Furthermore, the outer shell will be made of carbon fiber to ensure structural strength and low weight. And on the exterior, the width indicator lights for the cargo compartment, which are used to alert pedestrians. The internal storage space of the cargo hold should be able to accommodate at least 4 standard-sized goods in one shipment. The size of the goods is set at the smallest size of the current SF Express carton, which is 20cm*15cm*10cm. In order to meet the cargo capacity requirements of the Ark 150 unmanned aerial vehicle, it is necessary to ensure that the width and height of the cargo compartment are within 500mm, with no limit on the length.

2.4. Simulation Settings

This structure will undergo two simulation tests in different directions. These include a static structural simulation test for the load-bearing structure of the internal shelves and a fluid field simulation test for the cargo compartment shell.

The static structure simulation will use the software ANSYS 2022 R1. The simulation will be used to separately simulate the load-bearing test of the shelves. Static structure simulation of the shelves requires setting engineering data and selecting 6061 aluminium alloy. The model built in SolidWorks is imported into the geometry. 10mm grids are divided in the model, and standard Earth gravity, displacement, fixed support, and force are added under the static structure. The standard Earth gravity

is set vertically downward. Displacement and fixed support are set at the connection points of the shelves. A force of 25kg*9.81m/s^2=245.25N is applied at the place where the shelves hold goods. Under the solution, total deformation, equivalent (von-Mises) stress, equivalent strain and stress tools are added. In the stress tool, a safety factor is added.

The fluid field simulation will be carried out using the software COMSOL Multiphysics. The fluid field will be set to simulate the steady turbulent flow pattern for low-altitude flight. Define parameters in home:

$$Uinf = 17\ m/s. \tag{1}$$

$$rho = 1.225\ kg/m^3. \tag{2}$$

$$It = 0.05. \tag{3}$$

$$Lt = 0.1\ m. \tag{4}$$

$$k\_in = 1.5 * (Uinf * It)^2. \tag{5}$$

$$omega\_in = sqrt(k\_in)/((0.09)^{0.25} * Lt). \tag{6}$$

A wind tunnel was established in a geometry environment, and it was ensured to be far away from the model surface. For this simulation, a wind tunnel size of 3500mm (much larger than the length and width of the model) was adopted. Add materials to the wind tunnel: air. Add materials to the shell model: carbon fibre. Increase the inlet and outlet in the turbulent flow, k-ω (spf), set the normal plane of the air flow velocity as the inlet boundary, and set the velocity to Uinf. The exit boundary is set as the opposite side of the entrance, with a pressure of 0. Set the grid size to the default and add a boundary layer under the grid. Add two surface integrals under the derived value. Add two surface integrals under the derived value. Two datasets of surface integrals were selected for study 1, and the surface of the shell model was chosen. In this simulation, the direction of the velocity is along the positive z-axis. The first expression is set as: -spf.T_stressz, calculate the value of Fz. The second expression is:

$$(nz) * (nz > 0). \tag{7}$$

Calculate the value of Aref. Then add global calculations under the derived values and substitute the calculated values of surface integrals 1 and 2 into the formula:

$$Cd = Fz/(0.5 * rho * Uinf^2 * Aref). \tag{8}$$

Write this formula into the expression for the global calculation. And the wind resistance coefficient was calculated. Add a boundary probe under the derived value and replace its expression with: spf.T_t racz. Add a 3D drawing group under the result. Add surfaces and streamlines under the 3D drawing group. Set the expression for the surface as: spf.U. The unit is set to m/s. Set the number of flow lines to 1500, and the geometric entity layer to the surface of the shell model. Draw a three-dimensional drawing group and obtain a streamline diagram.

3. Result

3.1. 3D Modelling

To achieve the goal of a low drag coefficient, this shell is modelled after water droplets in nature and combined with actual conditions to meet the requirement of lower drag, can be seen in Figure 1. Compared to the conceptual design drawing, the actual shell has added some positions for the installation of the marker lights, and the bottom support structure in Figure 2. The opening method of this shell is an up-and-down sliding type. Inside, there is a screw rod and a motor for controlling the opening and closing of the shell. To meet the requirements of modular replaceable design, the part where the housing is connected to the unmanned aerial vehicle has reserved holes that can accommodate different screw installation positions and holes for connecting the wiring harness. The

material used is carbon fibre composite material, which features high strength, a lightweight design and excellent fatigue resistance. It perfectly matches the application scenario of the cargo hold shell.

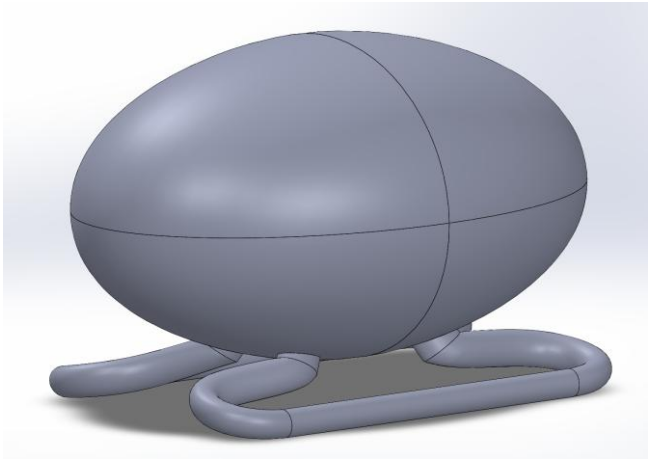

Figure 1. Conceptual design drawing of the shell (Picture credit: Original)

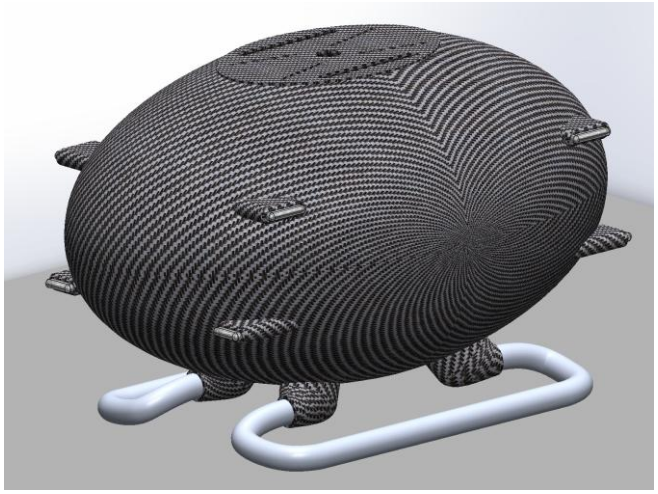

Figure 2. Final 3D model image of shell (Picture credit: Original)

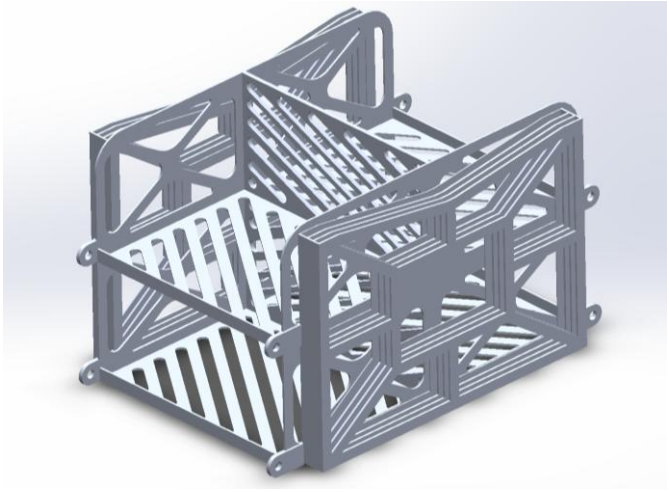

Figure 3. Final 3D model image of storage rack (Picture credit: Original)

The perforated design in Figure 3 of the shelves is to achieve sufficient lightweight design while meeting the required load-bearing capacity. While not affecting the structural strength and loading capacity, try to carry out hollowing-out designs for the structure to reduce its weight and leave more weight margin for carrying more cargo. While ensuring the structural strength and spatial dimensions, this shelf can accommodate 4 small-sized goods and 6 small-sized document envelopes. The size of

the document envelopes is set at the smallest size of the current SF Express document envelopes, which is 28.4cm*21.5cm.

3.2. Static structural simulation analysis

It can be seen from Figure 4 that the maximum deformation value is approximately 0.47 mm, while the minimum value is close to zero. The overall deformation range is very limited, indicating that the structure has a high overall stiffness and can maintain good shape stability under external loads.

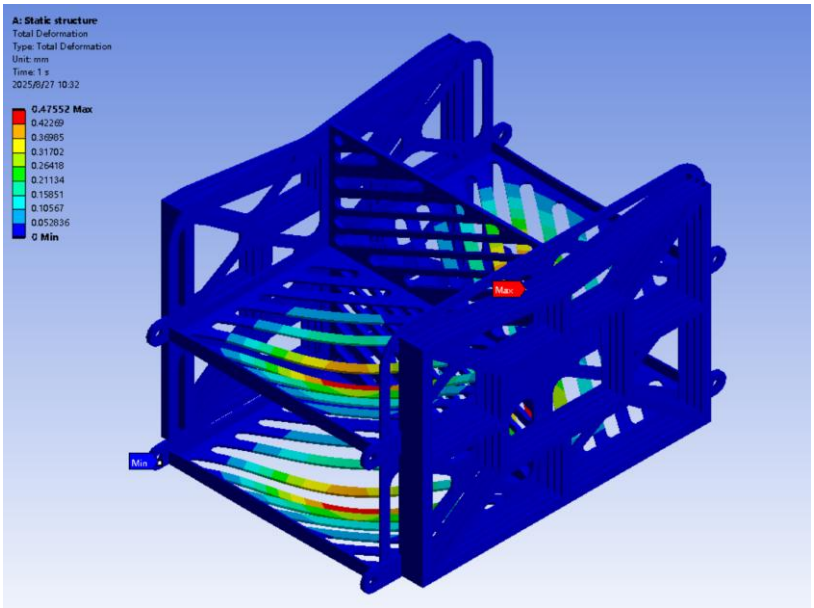

Figure 4. Total Deformation (Picture credit: Original)

The overall stress level is relatively low, with the maximum value being approximately 12.6 MPa in Figure 5, which is far below the yield strength of common 6061 aluminium alloy. This indicates that the structure has sufficient strength margin under the applied load conditions and has not approached the yield limit. The maximum stress is concentrated at the local connection points of the shelf and the areas where the shelf is subjected to the weight of the goods. The colour transitions from blue to yellow-green, and there are orange areas appearing locally. These positions are the convergence points of the force flow.

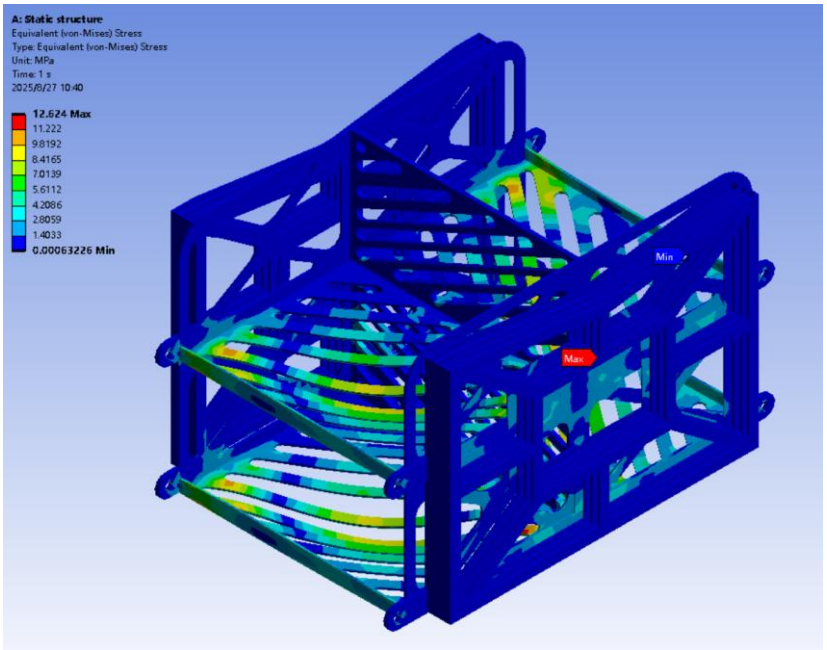

Figure 5. Equivalent (von-Mises) Stress (Picture credit: Original)

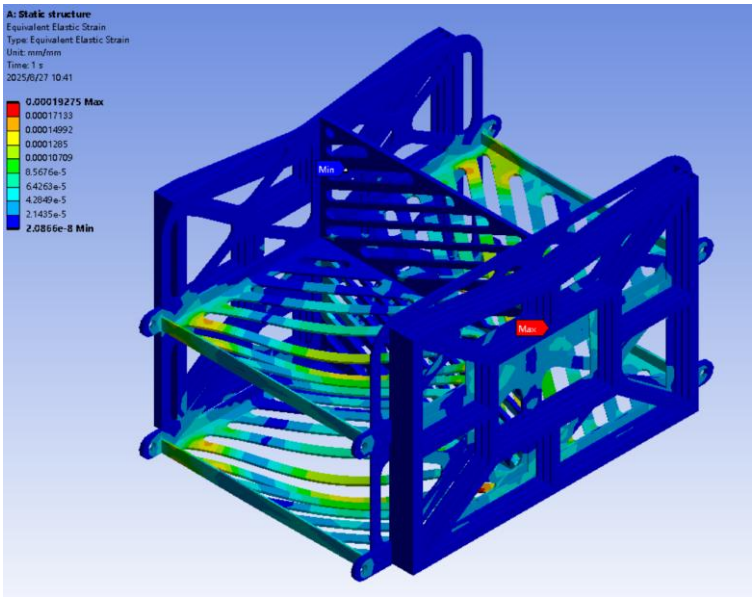

Figure 6. Equivalent Elastic Strain (Picture credit: Original)

By analysing the equivalent strain in Figure 6, the strain values of the overall structure are at a relatively low level. The maximum strain is approximately 1.9×10^(-4), and the minimum value is close to zero. This indicates that under the current load conditions, the structure is mainly in the small deformation elastic stage. The maximum value occurs at the connection point between the frame and the middle section. The colour transitions from blue to yellow and green, indicating that these positions have undergone significant deformation during the load transmission process. The overall structure of the shelves has sufficient rigidity and safety margin under the specified working conditions.

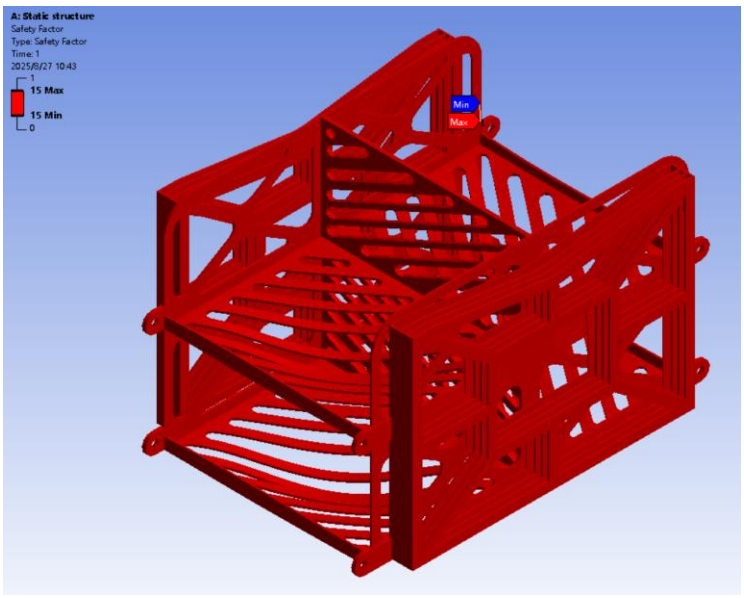

Figure 7. Safety Factor (Picture credit: Original)

Through simulation, it was found in Figure 7 that most areas of the overall structure of this shelf are at a high safety factor level (close to 15). The colours are basically the same, indicating that most of the structures have a relatively low stress level under the current load and sufficient strength margin. The overall structure remains within a high safety factor range, with no obvious dangerous points lower than 1. It can fully guarantee its cargo-carrying capacity and will not cause any safety issues.

3.3. Fluid Field Simulation Analysis

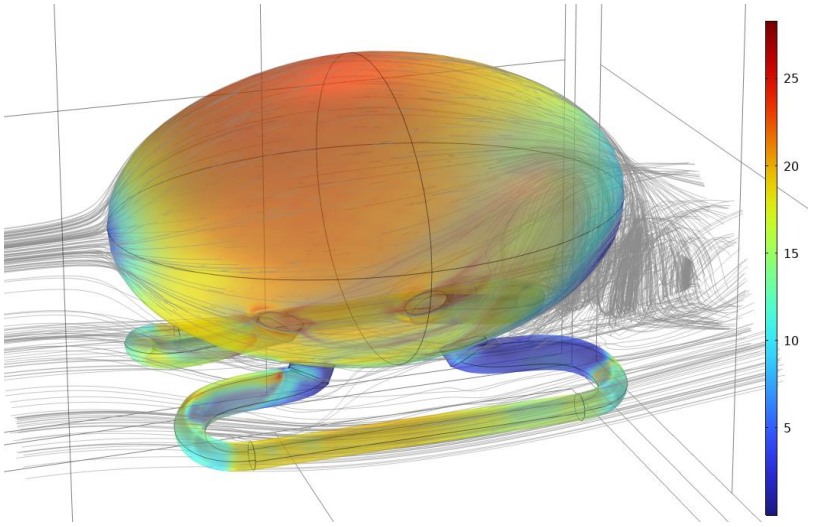

Figure 8. Surface streamline diagram (Picture credit: Original)

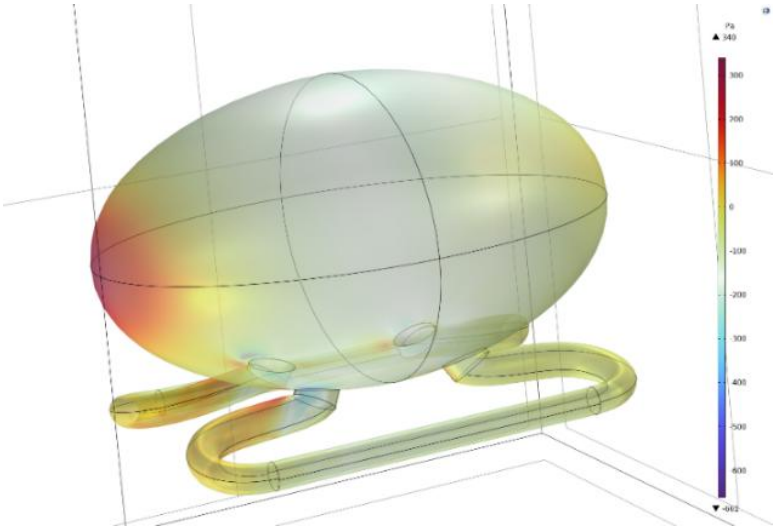

Figure 9. Surface pressure diagram (Picture credit: Original)

From Figure 8, it can be analysed that the leading-edge streamline is basically in close contact with the surface, while a distinct separation wake appears at the tail, accompanied by a wide recirculation zone and vortices. This will significantly increase the pressure difference resistance. The bottom support structure causes additional interference to the streamline of the upper part, resulting in a thicker and more asymmetrical wake.

The pressure generated in Figure 9 is the direct impact of the airflow, resulting in the conversion of dynamic pressure, and it is one of the main resistance sources. A distinct high-pressure area is formed at the front end of the shell, with a reddish colour and a pressure of approximately + 300 Pa. A large range of negative pressure appears in the rear of the shell and the trailing area of the support structure, with the lowest pressure being about - 600 Pa, indicating the presence of flow separation and vortex structures. The pressure distribution on the surface of the bottom support structure is complex, with alternating positive and negative pressures on the inner and outer sides, indicating that the support components significantly interfere with the main flow, which may lead to vortices and additional resistance.

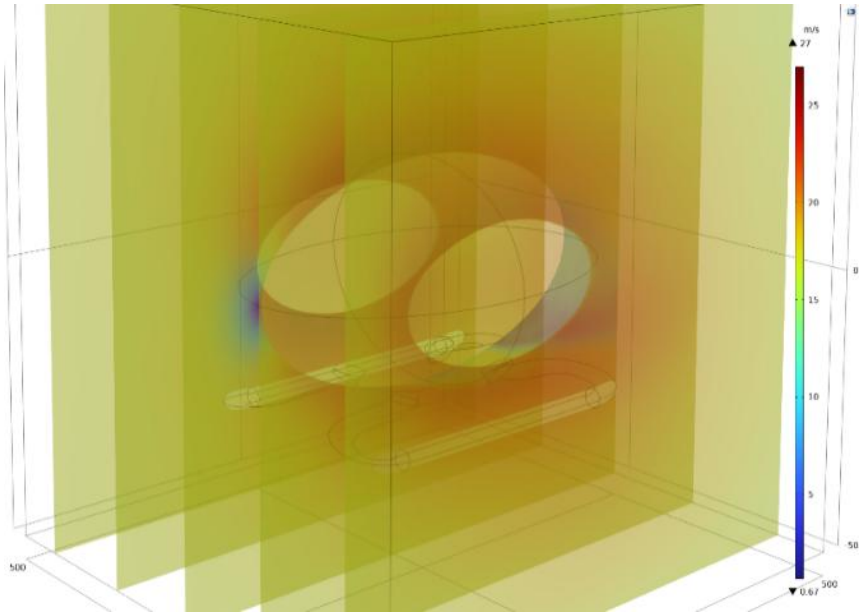

Figure 10. Speed distribution cloud chart (Picture credit: Original)

The speed range is between 0 and 27 m/s in Figure 10. Multiple slice sections are used to present the internal velocity gradient of the flow field, which can directly show the changes of the incoming flow in front of, behind and on both sides of the object. A distinct low-speed zone (blue-green) is formed in the front of the shell. The airflow is forced to flow around the supporting structures on both sides and at the bottom, and the local section shows an increase in speed (yellow-orange). There is a large range of speed reduction area (green-blue) at the rear of the object, which is significantly lower than the incoming flow speed, indicating the formation of flow separation and wake vortices.

In a turbulent flow, k-ω (spf) steady-state environment, the resistance force and the area of the resistance force on the shell were calculated, resulting in the numerical values Fz=8.2395 N and $Aref$=0.16458 m^2. Based on the wind resistance coefficient calculation formula:

$$Cd = Fz/(0.5 * rho * Uinf^2 * Aref). \quad (9)$$

The calculation result of the wind resistance coefficient for this shell is 0.28283. The wind resistance coefficient of the square cargo hold was simulated using the same method, which was 0.69109. The wind resistance coefficient of this square cargo compartment is also in line with that of a cube [7]. Although the wind resistance coefficient of water droplets in nature varies greatly, it can meet the wind resistance coefficient requirements of logistics drones, and compared with the square cargo hold, it has a significant improvement.

3.4. Structural Adaptability Analysis

The flow field results show that the cargo compartment shell forms a relatively high positive pressure area on the windward side, while generating a significant low-pressure area and a wide wake at the tail, resulting in a large pressure difference drag. The overall wind resistance coefficient of this shell is 0.28283, which is significantly higher than that of a square cargo hold. Compared with the claw-type loading method [8], this loading method adds a rectifying shell to the outside of the goods. This will not only save more energy during flight but also enhance the aircraft's ability to withstand sudden gusts. The maximum pressure difference reaches approximately ± 300 - 600 Pa. The velocity loss in the wake area is significant, indicating that the shell has not fully achieved a streamlined design. The bottom support structure interferes with the main flow, inducing local separation and vortices, further increasing the total drag. This will limit the aerodynamic efficiency of the cargo compartment shell during high-speed cruise conditions, potentially affecting the range and endurance of the unmanned aircraft. The improvement directions include optimizing the aft edge contraction ratio of

the shell, adding transition surfaces, and streamlining or installing fairings on the bottom support components to reduce drag [9].

Under the static load condition, the stress level of the shelves is relatively low, with the maximum equivalent stress being approximately 12.6 MPa, which is far below the allowable stress of common 6061 aluminium alloy. The equivalent strain value is at the order of 10^{-4}, and the total deformation is approximately 0.47 mm, indicating that the overall structure has a high strength and stiffness margin, and can stably carry the goods. Compared with the loading structure that requires dedicated cargo containers [10], this loading structure is more suitable for loading goods of various sizes and multiple pieces. The safety factor distribution is close to 15, indicating that the material utilization is insufficient, some structural components and the outer frame have redundant stiffness, and there is room for weight reduction optimization. The stress concentration areas mainly occur at the connection points and the crossbeams, and attention should be paid to long-term fatigue and connection reliability.

4. Conclusion

This paper designs a modular loading structure for logistics drones and reimagines and designs the shells of the existing square cargo compartments and the similar-shaped cargo compartments. COMSOL Multiphysics 6.3 conducted a numerical simulation of a three-dimensional cargo hold shell model under the turbulent k-ω model. The system calculated the aerodynamic drag and wind resistance coefficient under the inflow speed of 17 m/s. Through reasonable settings such as the calculation domain and boundary conditions, the numerical results were well-converged. The wind resistance coefficient of the square cargo hold was compared, and an improvement in the wind resistance coefficient was obtained. The shelves inside the cargo hold were designed for small goods, enabling the loading of 4 small goods and 6 small envelopes. The shelves were simulated for static structure using ANSYS 2022 R1, and the results showed high strength and stiffness margins. In summary, the cargo hold and shelf structure can meet the safety and load-bearing requirements, but there is still significant room for optimization in terms of aerodynamic efficiency and lightweighting.

Future optimization research can be conducted in the following aspects: Carry out aerodynamic optimization by means of aft body contraction, fairing design or streamline treatment of support components to reduce the wake range and pressure difference resistance, and optimize the cargo compartment shape of the system. Carry out topological optimization or material substitution research on the shelves, reducing redundant mass while maintaining strength and stiffness, and improving material utilization.

References

[1] Liu Guangwei, Mao Rong, Lu Jianming. Research on the Development of Low-altitude Economy Driven by Unmanned Aerial Vehicle Technology. Engineering Economics. 2025, 44 (22): 157-160.

[2] Editorial Department of This Journal. Focusing on the "Logistics Voice" at the National Two Sessions, Paying Attention to New Hotspots in the Development of the Logistics Industry. Logistics Technology and Application. 2025, 30 (04): 52-57.

[3] Li Bingyi, Sun Fuqi. Listening to a Tea Party on "The Future of Logistics". China Logistics. 2025, (05): 9-17.

[4] Zhu Yonglin. Research on the Innovation of Logistics Industry in the Context of Low-Cost Economy, China Industrial News. 2025, 017.

[5] Zhang Shixuan. Review of the Current Development Status of Logistics Drones. Internal Combustion Engine and Accessories. 2020, (08): 99-101.

[6] Liu Jia Shi. Research on the Design and Optimization of Drone Logistics Network for B2C E-commerce Enterprises (Master's Degree Dissertation, Beijing Jiaotong University). Master's Degree. 2021.

[7] Khan, M. H., Parvez, K., Islam, M. Q., Rahman, M. M. Flow around a cube for Reynolds numbers between 5000 and 40,000. Journal of Naval Architecture and Marine Engineering. 2018, 15 (1): 13–22.

[8] Su Jiyang. Design of Multi-UAV for Logistics Based on Arduino. Mechanical and Electrical Engineering Technology. 2023, 52 (11): 259-261+299.

[9] Rao, H., Chen, Y., Shi, Y., Yang, T., Liu, H. Adjoint-Based Aerodynamic Design Optimization and Drag Reduction Analysis of a Military Transport Aircraft Afterbody. Aerospace. 2023, 10 (4): 331.

[10] Chen Li, He Yiming, Bao Hongwen, Deng Zengqi. Hardware Integration Design of Unmanned Aerial Vehicles for Logistics Scenarios. Logistics Engineering and Management. 2025, 47 (04): 1-5+13.